OPTIMIZATION OF A WIDE-FIELD EDDY CURRENT PROBE USING A BOUNDARY ELEMENT METHOD BASED MODEL

Jay M. Amos and Joseph C. Chao*

United Technologies, Pratt & Whitney
P.O. Box 109600, M/S 707-21 *
W. Palm Beach, FL 33410

INTRODUCTION

Eddy current (EC) methods are widely used in the NDE inspection of critical aircraft engine components. Assessment of these components is particularly challenging due to the use of low conductivity materials and small flaw sizes, driven by high performance designs. Diverse EC probe designs have been produced over the years to maximize defect sensitivity, depending on the flaw characteristics and material type and condition. Traditionally, the performance of an eddy current probe design is evaluated by fabricating numerous prototype probes and performing scans in the desired test condition. Clearly this approach is both time-consuming and expensive. In particular, the EC probe has to be reconstructed each time the probe design is changed, and one design cycle may require a number of iterations before satisfactory performance is achieved. Moreover, due to the inexact science of probe fabrication, the performance of small design changes may be disguised by changes in manufacturing process variables.

A more economical alternative to this development cycle is to evaluate the design parameters through the use of numerical simulation [1] - [3]. This process is conceptually simple and cost-effective whereas the design changes are done in a computer aided design (CAD) environment. The probe performance may be evaluated based on the interrogating electromagnetic (EM) fields produced by the designed probe which can be easily calculated using the boundary element method (BEM) at desired locations. By casting the entire EC inspection process in terms of a numerical model, impedance changes due to the flaw response can be generated by computing the solutions to the integral equations.

This paper describes the use of a BEM-based EC modeling package in optimizing a reflective wide field element design. Specifically, the design parameter under consideration is the width of the pancake receiver gap and the effect of driver and receiver separation. For this problem, the EC model will be used to numerically predict the variation in flaw responses as the receiver gap width varies. The optimization process is achieved by selecting the design that produces the most sensitive flaw response. The BEM

* Now at AlliedSignal Engines, P.O. Box 52181, M/S 301-227, Phoenix, AZ 85072

Review of Progress in Quantitative Nondestructive Evaluation, Vol 17
Edited by D.O. Thompson and D.E. Chimenti, Plenum Press, New York, 1998

has advantages in that it is not constrained by geometrical singularities such as edges, corners and cracks, and it permits arbitrary shapes for the part, probe, cores and windings.

BOUNDARY ELEMENT METHOD

Over the years, several numerical methods have been applied to solve eddy current inspection problems. These techniques include both the finite element methods and the volume integral methods [4] - [7]. However, there are a number of reasons why one would prefer to numerically solve the boundary integral equations (BIEs) as oppose to solve the differential equations (DEs) or the volume integral (VI) equations. First, in the case of BIEs, the unknown variables are expressed in terms of equivalent source densities that exist only on the bounding surfaces of the problem geometries. In contrast, the unknowns to the DEs are the actual field or potential variables that exist everywhere in the problem domain. In the case of the VI approach, the unknown density functions are defined volumetrically. Naturally, the number of unknowns are significantly less in the BIE governed problem than the other two approaches. Second, since the modeled problem requires simulating the scanning process, no remeshing is needed for the BIE problem. However, remeshing is required for the DE case as the probe moves relative to the test component.

The proposed BEM-based electromagnetic modeling software accepts input from standard CAD packages such as IDEAs™ and PATRAN™. The CAD inputs describe both the geometrical and mesh connectivity information of the problem. This description includes the eddy current probe design, the specimen under inspection and the crack morphology. Additional information such as the operating frequency and material properties are provided to the model for computation. Using these inputs the BEM model then computes the resulting electromagnetic disturbance caused by the presence of the crack. The severity of the disturbance is quantified in terms of impedance changes from the crack case to the uncracked case. With a solution to the forward model from the model, this tool could easily be incorporated into a POD model for predicting and improving the inspection POD.

BOUNDARY INTEGRAL EQUATIONS

For a given general eddy current inspection problem, the test specimen can assume an arbitrary shape, including geometrical singularities such as edges. The model utilizes a variational form of the Hertzian potential approach by defining the total magnetic fields in the air region outside the specimen as

$$\vec{H} = \vec{H}^{(0)} + \nabla\phi \tag{1}$$

with the quasistatic approximation

$$\nabla^2\phi = 0 \tag{2}$$

where

$\vec{H}$ = Total magnetic fields in the air region,
$\vec{H}^{(0)}$ = Incident magnetic fields in the absence of the test specimen, and
ϕ = Scalar magnetic potential function.

Internal to the conductive specimen, the total magnetic field is defined as

$$\vec{H} = \vec{h} + \nabla\phi \tag{3}$$

where $\vec{h}$ is an auxiliary vector potential function. At the air/specimen interface, the normal component of the magnetic flux density and the tangential components of the magnetic fields are continuous across the boundary.

$$\left(\vec{H} - \nabla\phi\right)_t = \vec{H}_t^{(0)} = \vec{h}_t \tag{4}$$

With the quasistatic approximation, the kernel function in the air region can assumed to be static, $\overline{G}$, while the kernel function inside the conductive specimen remains dynamic, G. Consequently, collocating on the specimen surface yields four BIEs.

$$\int_{S_H} \left(-\partial_n G\right)\phi + \left(\partial_n G_o\right)\phi_p + G\left(\mu^{-1}B_n - h_n\right) dS = 0 \tag{5}$$

$$\int_{S_H} \left\{-\partial_n\left(G - G_o\right)\right\}\phi + G\left(\mu^{-1}B_n - h_n\right) - G_o\left(\mu_o^{-1}B_n - H_n^{(0)}\right) dS = 0 \tag{6}$$

$$\hat{n}_p \cdot \int_{S_H} \left\{\nabla\left(G - G_o\right)\right\} \times \left(\hat{n} \times \vec{H}^{(0)}\right) - \left(\nabla G\right)h_n + \left(\nabla G_o\right)H_n^{(0)} + \left(\nabla G_o\right)\left(h_n - H_n^{(0)}\right) - k^2 G\left(\frac{\hat{n} \times \vec{E}}{j\omega\mu} - \hat{n}_q\phi\right) dS = 0 \tag{7}$$

$$\hat{n}_p \times \int_{S_H} \left\{\nabla\left(G - G_o\right)\right\} \times \left(\hat{n} \times \vec{H}^{(0)}\right) - \left(\nabla G\right)h_n + \left(\nabla G_o\right)H_n^{(0)} - k^2 G\left(\frac{\hat{n} \times \vec{E}}{j\omega\mu} - \hat{n}_q\phi\right) dS = 0 \tag{8}$$

Equations (5) through (8) constitute the governing boundary integral equations (BIEs) of the EC inspection problem, in the absence of cracks. For the crack case, several of the above equations must be modified and collocation on the crack surface needs to take place.

CRACK FORMULATION

Crack modeling is a fascinating topic that has captured significant interests from many researchers. Over the years, many methodologies have been proposed to model the eddy current response from tight cracks. In the application of boundary integral equations approach, a common practice is to model the eddy current discontinuity across the crack surface as a distribution of dipole potential source function. The potential functions are coupled with the governing equations associated with the other surfaces before the numerical solution is computed. It can be shown that the BIEs for the specimen and the crack are

$$\int_{S_H} \left(-\partial_n G\right)\phi + \left(\partial_n G_o\right)\phi_p + G\left(\mu^{-1}B_n - h_n\right) dS = 0 \tag{9}$$

$$\int_{S_H} \left\{-\partial_n\left(G - G_o\right)\right\}\phi + G\left(\mu^{-1}B_n - h_n\right) - G_o\left(\mu_o^{-1}B_n - H_n^{(0)}\right) dS = 0 \tag{10}$$

$$\hat{n}_p \cdot \int_{S_H} \left\{\nabla(G-G_o)\right\}\times\left(\hat{n}\times\vec{H}^{(0)}\right)-(\nabla G)h_n+(\nabla G_o)H_n^{(0)}+(\nabla G_o)\left(h_n-H_n^{(0)}\right)$$
$$-k^2 G\left(\frac{\hat{n}\times\vec{E}}{j\omega\mu}-\hat{n}_q\phi\right)dS+\hat{n}_p\cdot\int_{S_k}G\left(\hat{n}_q\times\nabla\varphi(q)\right)=0 \tag{11}$$

$$\hat{n}_p\times\int_{S_H}\left\{\nabla(G-G_o)\right\}\times\left(\hat{n}\times\vec{H}^{(0)}\right)-(\nabla G)h_n+(\nabla G_o)H_n^{(0)}-k^2G\left(\frac{\hat{n}\times\vec{E}}{j\omega\mu}-\hat{n}_q\phi\right)dS$$
$$+\hat{n}_p\times\int_{S_k}G\left(\hat{n}_q\times\nabla\varphi(q)\right)=0 \tag{12}$$

$$-j\omega\mu_h\int_{S_H}\hat{n}_p\cdot\left[(\nabla G)\times\left(\tfrac{-\hat{n}\times\vec{E}}{j\omega\mu}+\hat{n}\phi(q)\right)\right]dS-j\omega\mu_h\int_{S_k}\hat{n}_p\cdot\hat{n}_q G\varphi(q)\,dS$$
$$-\frac{1}{\sigma}\int_{S_k}\tfrac{\partial^2 G}{\partial n_p\partial n_q}\varphi(q)\,dS=j\omega\mu_h\int_{S_k}\hat{n}_p\cdot K\vec{H}_t^{(0)}(q)\,dS \tag{13}$$

where

$$K_{ij}=\delta_{ij}G+\tfrac{1}{k^2}\tfrac{\partial^2(G-\bar{G})}{\partial x_i\partial x_j} \tag{14}$$

and σ = conductivity of the test specimen.

It should be noted that a line integral over the mouth of the crack has been absorbed into the surface integral in equation (26) through the use of Stoke's theorem. A more detailed discussion on this derivation can be found in [8].

EXPERIMENT

In order to begin a validation of the reflection model with probes of this type, the model results were qualitatively compared with the experimental results in several cases. For this problem, only the air-cored reflection probe is considered. The geometry of the probe is first designed in a CAD description with design variations of interest. Next, the specimen geometry and the crack morphology are defined so the geometrical location of the probe relative to the specimen and the crack is properly accounted. Test conditions are described in Table 1 for two crack sizes of interest. In this evaluation the probe is scanned over a specimen with a crack centered under the element. Next, the output of the CAD description is fed to the BEM-based model to compute the unknown density functions at the specimen and crack surfaces. Once the solution is obtained, one can compute the impedance change by applying Auld's reciprocity theorem using the surface solutions of the two cases of with and without the presence of the crack. The reciprocity equation for the differential reflection probe is

$$\Delta Z=\tfrac{-1}{I_T}\int_{S_K}\left(\tfrac{1}{I_{R1}}\vec{E}_{R1}^{(0)}-\tfrac{1}{I_{R2}}\vec{E}_{R2}^{(0)}\right)\cdot\hat{n}\varphi_T(q)\,dS_q \tag{15}$$

Where the subscripts T, R1, R2 represents the response from exciting the probe with the driver, receiver #1 and receiver #2, respectively.

All of the results shown here are in titanium with a probe frequency of 4 MHz. The element is scanned in 0.2 mm steps with the flaw parallel to the scan direction. To compute the impedance change requires about 4 hours running on a 256 MHz Alpha workstation. Fig. 1 illustrates an experimental result and two modeled results for one coil

Table I. Test parameters

	Element Dimension (mm)	Liftoff (mm)	Mesh Nodes	Crack size, dp. x lng. (mils)	Crack Mesh Nodes	μ (e-6 H/m)	σ (e6 S/m)	Part Mesh Nodes
Driver	3.3 long x 0.457 high	0.15	128	6 x 12 11 x 22	57	1.2566	0.6135	193
Pancake Receiver	3.3 long single layer	0.302	576					

design with similar receiver gap widths. In this case it appears the model result using 0.020" gap compares much better to the real result than the modeled 0.026" gap. This disparity may be due to inaccuracy of the measured probe gap dimension of 0.025" that varies somewhat across the element width. Real and imaginary traces are shown in Fig. 2.

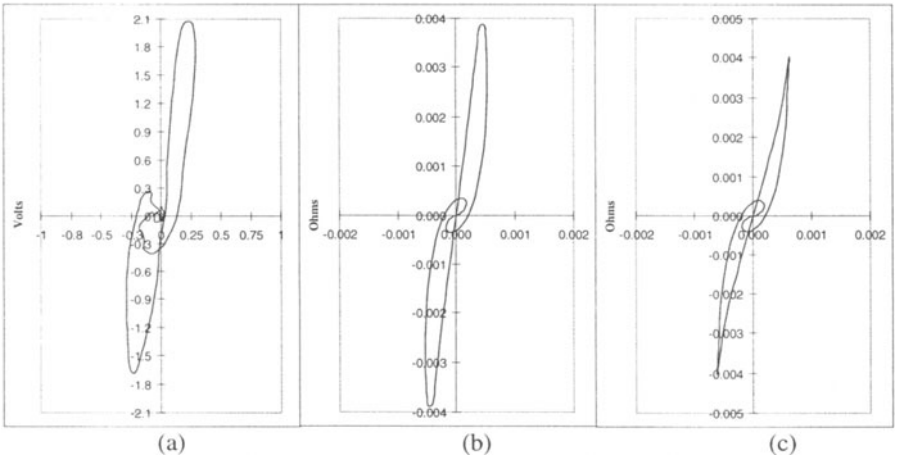

Figure 1. Comparison of measured and numerical results, a) measured induced voltage w/0.025" gap, b) modeled impedance w/0.020" gap, c) modeled impedance w/0.026" gap.

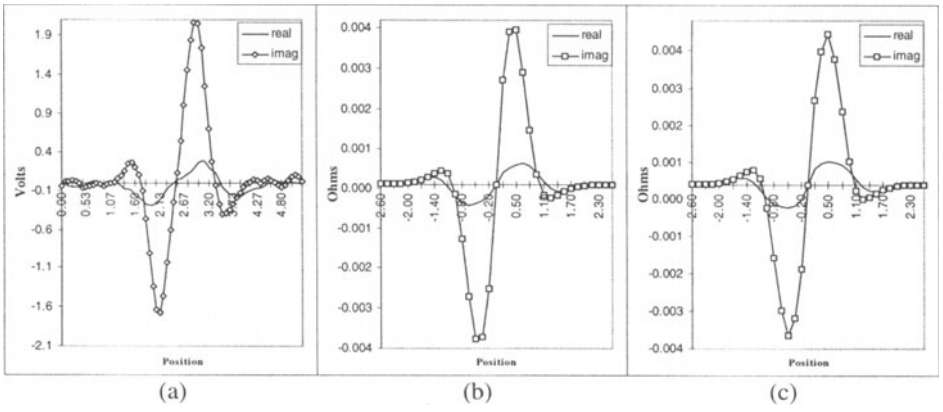

Figure 2. Comparison of measured and numerical results, a) measured signal w/0.025" gap, b) modeled signal w/0.020" gap, c) modeled signal w/0.026" gap.

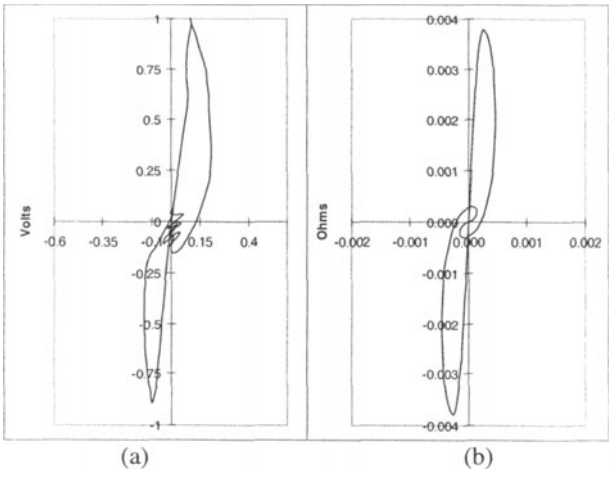

Figure 3. Comparison of measured and numerical results, a) measured induced voltage w/0.015" gap, b) modeled impedance w/0.014" gap.

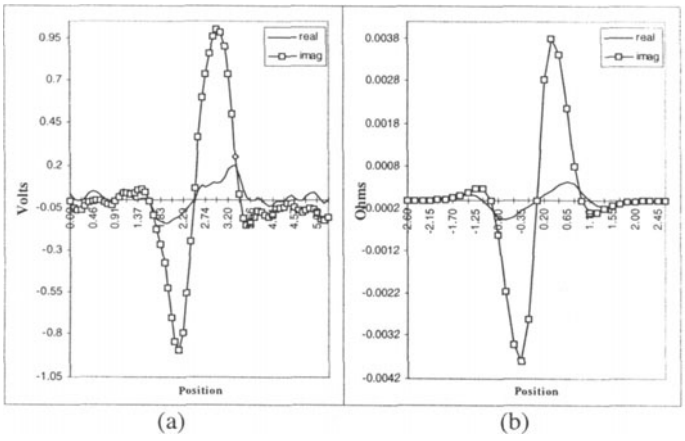

Figure 4. Comparison of measured and numerical results, a) measured signal w/0.015" gap, b) modeled signal w/0.014" gap.

The comparison of experimental and modeled results is shown for another design case in Fig. 3. Good agreement can be seen between the actual receiver gap width of 0.015" and the modeled result with a gap of 0.014" with otherwise identical design parameters. The real and imaginary channel responses are shown in Fig. 4.

DESIGN OPTIMIZATION USING THE BEM MODEL

Using numerical simulations a probe design may be easily optimized and effects of fabrication process variables can be quantified. One critical design variable of interest was in optimizing the gap width in the pancake receiver. From the modeled impedance results shown in Fig. 5 one can see an optimal receiver gap for this probe type of between 0.026" and 0.030" for this range of flaw sizes. The receiver gaps evaluated in the model varied from 0.007" to 0.045" in width. This provides critical design process information without extensive time and costs of probe fabrication.

Positioning of the driver above the receiver during fabrication is subject to a number of variables that can influence probe sensitivity. The driver may be tilted with respect to the receiver and inspection surface that may affect probe uniformity. Also, separation of the driver and receiver is dictated by the thickness of the epoxy used to attach the receiver. Fig. 6 illustrates the effect of increasing driver/receiver separation beginning at 0.003" (representing a thin epoxy). As this separation increases as it might with excessive epoxy buildup, the signal decreases 11.5% with an additional 0.003" separation, and another 10.9% for additional 0.004" separation. Now, the effect of such process variables can be understood to quantify design tolerances and focus quality efforts for EC probes.

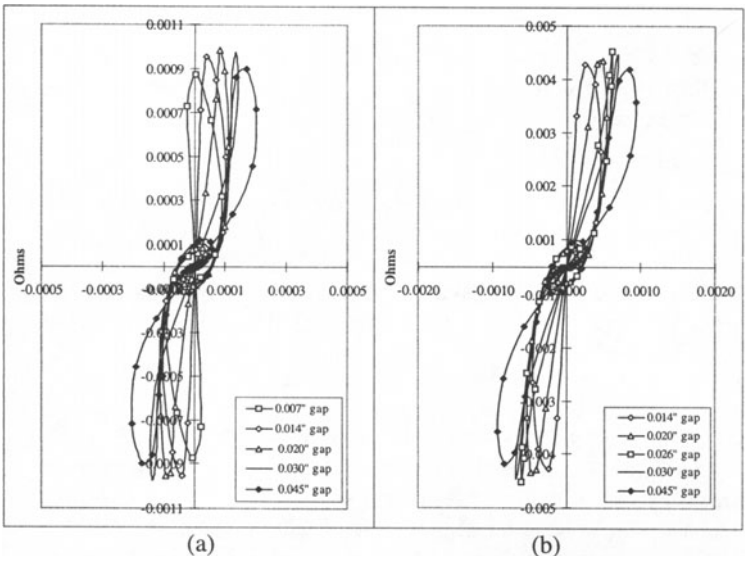

Figure 5. Model results of parallel scan with varying receiver gap, a) over a 0.006" x 0.012" long crack, b) over a 0.011" x 0.022" long crack

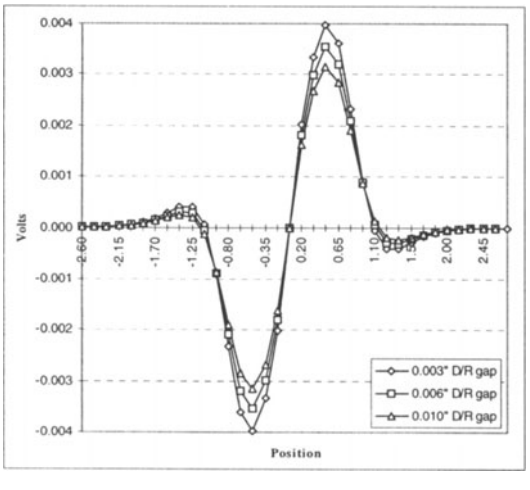

Figure 6. Modeled signal response with variation in driver/receiver separation.

CONCLUSIONS

BEM EC modeling can effectively assist probe design in optimizing certain parameters to reduce development time and cost. Reflection modes in either absolute or differential configuration have recently been incorporated into the BEM-based simulator code. Reasonable agreement was found with predicted impedance results and experimentally measured from an eddy current instrument. Future efforts will include the quantitative validation of the transmit-receive BEM modeling code along with an extension of the formulation to allow ferromagnetic cores.

ACKNOWLEDGMENTS

This work was supported primarily by the Engine Titanium Consortium, In-Service Eddy Current Inspection task through a grant from the Federal Aviation Administration.

REFERENCES

1. N. Nakagawa, J. Chao, and A.N.S. Prasad, "In-Service Eddy Current Inspection and Computer Simulation", in *Nondestructive Testing of Materials,* eds. R. Collins, W.D. Dover, J.R. Bowler, and K. Miya (IOS Press, 1995), p.203.
2. J. Chao, A.N.S. Prasad, N. Nakagawa, and D. Raulerson, "Computer Assisted Eddy Current Probe Design", in *Review of Progress in QNDE,* Vol. 15, eds. D.O. Thompson, D.E. Chimenti (Plenum Press, 1996), p.1105.
3. N. Nakagawa and J. Chao, "Extended magnetic potential method for quasi-static electromagnetism and eddy current phenomena", in *Review of Progress in QNDE,* Vol. 15, eds. D.O. Thompson, D.E. Chimenti (Plenum Press, 1996), p.339.
4. W. S. Dunbar, "The Volume Integral Method of Eddy Current Modeling," *J. Nondestructive Eval.,* Vol. 5, pp 9-14, 1985.
5. W. S. Dunbar, "The Volume Integral Method of Eddy Current Modeling:Verification," *J. Nondestructive Eval.,* Vol. 7, pp 43-54, 1988.
6. W. Lord, Y. Sun, S. Udpa and S. Nath, "A Finite Element Study of the Remote Field Eddy Current Phenomenon," *IEEE Trans. On Magnetics,* Vol. 24, No. 1, pp 435-438, January 1988.
7. Y. Sun, "Finite Element Study of Diffusion Energy in Low Frequency Eddy Current Fields," *Materials Evaluation,* Vol. 47, pp 87-92, January 1989.
8. J.R. Bowler, "Eddy Current Interaction with an Ideal Crack," *J. of Applied Physics,* Vol. 75, pp 8128-8137, June 1994.